Tunneling dynamics and band structures of three weakly coupled Bose-Einstein condensates

Qiuyi Guo,[1] **XuZong Chen,**[1] **and Biao Wu**[2,3,*]

[1]*Institution of Quantum Electronics, School of Electronics Engineering & Computer Science, Peking University, Beijing 100871, China*
[2] *International Center for Quantum Materials, Peking University, Beijing 100871, China,*
[3] *Collaborative Innovation Center of Quantum Matter, Beijing 100871, China*
[*] *wubiao@pku.edu.cn*

Abstract: We study the tunneling dynamics and energy bands of three Bose-Einstein condensates which are coupled weakly with each other. The study is carried out with both the mean-filed model and the second-quantized model. The results from these two models are compared and found to agree with each other when the particle number is large. Without interaction, this system possesses a Dirac point in its energy band. This Dirac point is immediately destroyed and develops into a loop structure with arbitrary small interaction. This loop structure has a strong effect on the tunneling dynamics. We find that the tunneling dynamics in this system is very sensitive to the system parameter, e.g., the interaction strength. This sensitivity is found to be caused by the chaos in the mean-field model and the avoided energy crossings with tiny gaps in the second-quantized model. This result gives a certain indication on how the classical dynamics and quantum dynamics are connected in the semi-classical limit. Our mean-field results are also valid for three mutually coupled optical nonlinear waveguides.

OCIS codes: (020.1475) Bose-Einstein condensates; (140.1540) Chaos.

References and links

1. M. H. Anderson, J. R. Ensher, M. R. Matthews, C. E. Wieman, and E. A. Cornell, "Observation of Bose-Einstein condensation in a dilute atomic vapor," Science **269**, 198–201 (1995).
2. C. C. Bradley, C. A. Sackett, J. J. Tollett, and R. G. Hulet, "Evidence of Bose-Einstein condensation in an atomic gas with attractive interactions,"Phys. Rev. Lett. **75**, 1687–1690 (1995).
3. I. Bloch,"Ultracold quantum gases in optical lattices," Nature Phys. **1**, 23–30 (2005).
4. M. Greiner, O. Mandel, T. Esslinger, T W. Hänsch and I. Bloch,"Quantum phase transition from a superfluid to a Mott insulator in a gas of ultracold atoms," Nature(London)**415**, 39–44 (2002).
5. J. v. Porto, "Optical lattices: More than a look," Nature Phys. **7**, 280–281 (2011).
6. D. Jaksch, C. Bruder, J. I. Cirac, C. W.Gardiner, and P. Zoller, "Cold Bosonic Atoms in Optical Lattices, " Phys. Rev. Lett. **81**, 3108–3111 (1998).
7. L.M. Duan, E. Demler, and M. D. Lukin, "Controlling spin exchange interactions of ultracold atoms in optical lattices ," Phys. Rev. Lett. **91**, 090402 (2003).
8. Y. Shin, M. Saba, A. Schirotzek, T. A. Pasquini, A. E.Leanhardt, D. E.Pritchard, and W. Ketterle, "Distillation of Bose-Einstein condensates in a double-well potential," Phys. Rev. L **92**, 150401 (2004).
9. M. J. Steel and M. J. Collett,"Quantum state of two trapped Bose-Einstein condensates with a Josephson coupling," Phys. Rev. A. **57**, 2920–2930 (1998).

#211632 - $15.00 USD Received 8 May 2014; revised 16 Jul 2014; accepted 17 Jul 2014; published 31 Jul 2014

10. M. Albiez, R. Gati, J. Fölling, S. Hunsmann, M. Cristiani, and M. K. Oberthaler, "Direct observation of tunneling and nonlinear self-trapping in a single Bosonic Josephson junction ," Phys. Rev. Lett. **95**, 010402 (2005).
11. Y. A. Chen, S. D.Huber, S. Trotzky, I. Bloch and E. Altman, "Many-body LandauZener dynamics in coupled one-dimensional Bose liquid ," Nature Phys. **7**, 61-67 (2011).
12. B. Wu and Q. Niu, "Nonlinear Landau-Zener tunneling," Phys. Rev. A. **61**, 023402 (2000).
13. J. Liu, B. Wu, and Q. Niu, "Nonlinear evolution of quantum states in the Adiabatic regime," Phys. Rev. Lett. **90**, 170404 (2003).
14. B. Wu and Q. Niu, "Superfluidity of BoseEinstein condensate in an optical lattice: LandauZener tunnelling and dynamical instability," New J. Phys. **5**, 104.1-104.24 (2003).
15. C. Kasztelan, S. Trotzky, Y.A. Chen, I. Bloch, I. P. McCulloch, U. Schollwock, and G. Orso,"Landau-Zener Sweeps and Sudden Quenches in Coupled Bose-Hubbard Chains," Phys. Rev. Lett. **106**, 155302 (2011).
16. G. J. Milburn, J. Corney, E. M. Wright, and D. F. Walls, "Quantum dynamics of an atomic Bose-Einstein condensate in a double-well potential," Phys. Rev. A **55** 4318–4324 (1997).
17. L. Pitaevskii and S. Stringari, "Thermal vs quantum decoherence in double well trapped Bose-Einstein condensates," Phys. Rev. L **87** 180402 (2001).
18. Y. Shin, M. Saba, T. A. Pasquini, W. Ketterle, D. E. Pritchard, and A. E. Leanhardt, "Atom interferometry with Bose-Einstein condensates in a double-well potential," Phys. Rev. L **92**, 050405 (2004).
19. K. Maussang, G. E. Marti, T. Schneider, P. Treutlein, Y. Li, A. Sinatra, R. Long, "Enhanced and Reduced Atom Number Fluctuations in a BEC Splitter," J. Estéve and J. Reichel, Phys. Rev. Lett. **105**, 080403 (2010).
20. A. Sinatra, Y. Castin and Y. Li, "Particle number fluctuations in a cloven trapped Bose gas at finite temperature," Phys. Rev. A **81**, 053623 (2010).
21. B. Wu and J. Liu, "Commutability between the Semiclassical and Adiabatic Limits," Phys. Rev. L **96**, 020405 (2006).
22. X. B. Luo, Q. T. Xie, and B. Wu, "Nonlinear coherent destruction of tunneling," Phys. Rev. A **76**, 051802 (2007).
23. H. Pu, W. P. Zhang, and P. Meystre, "Macroscopic Spin Tunneling and Quantum Critical Behavior of a Condensate in a Double-Well Potential," Phys. Rev. L **89** 090401 (2002).
24. A. Smerzi, S. Fantoni, S. Giovanazzi, and S. R. Shenoy, "Quantum Coherent Atomic Tunneling between Two Trapped Bose-Einstein Condensates," Phys. Rev. Lett. **79**, 4950-4953 (1997).
25. B. P. Anderson, P. C. Haljan, C. A. Regal, D. L. Feder, L. A. Collins, C. W. Clark, and E. A. Cornell, "Watching Dark Solitons Decay into Vortex Rings in a Bose-Einstein Condensate," Phys. Rev. Lett. **86**, 2926-2929 (2001).
26. S. Aubry, S. Flach, K. Kladko, and E. Olbrich, "Manifestation of classical Bifurcation in the spectrum of the integrable quantum dimer," Phys. Rev. Lett. **76**, 1607-1610 (1996).
27. Q. Thommen, J. C. Garreau, and V. Zehnle, "Classical chaos with Bose-Einstein condensates in tilted optical lattices," Phys. Rev. Lett. **91**, 210405 (2003).
28. J. A. Stickney, D. Z. Anderson, and A. A. Zozulya, "Transistorlike behavior of a Bose-Einstein condensate in a triple-well potential," Phy. Rev. A. **75**, 013608 (2007).
29. R. Franzosi, V. Penna, R. Zecchina, "Quantum dynamics of coupled bosonic wells within the Bose-Hubbard picture," Mod. Phys. B **14**, 943–961 (2000).
30. L. Amico and V. Penna, "Dynamical Mean Field Theory of the Bose-Hubbard Model," Phys. Rev. Lett. **80**, 2189–2192 (1998).
31. R. Paredes, "Tunneling of ultracold Bose gases in multiple wells," Phys. Rev. A **73**, 033616 (2006).
32. S. Mossmann, and C. Jung, "Semiclassical approach to Bose-Einstein condensates in a triple well potential," Phys. Rev. A **74**, 033601 (2006).
33. J. A. Stickney, D. Z. Anderson, and A. A. Zozulya, "Transistorlike behavior of a Bose-Einstein condensate in a triple-well potential," Phys. Rev. A **75**, 013608 (2007).
34. F. Trimborn, D. Witthaut and H. J. Korsch, "Beyond mean-field dynamics of small Bose-Hubbard systems based on the number-conserving phase-space approach," Phys. Rev. A **79**, 013608 (2009).
35. P. Buonsante, R. Franzosi and V. Penna, "Persistence of mean-field features in the energy spectrum of small arrays of BoseEinstein condensates," J. Phys. B. **37**, S229-238 (2004).
36. L. Cao, I. Brouzos, S. Zllner, and P. Schmelcher, "Interaction-driven interband tunneling of bosons in the triple well ," New J. Phys. **13**, 033032 (2011).
37. E. M. Graefe, H. J. Korsch, and D. Witthaut, "Mean-field dynamics of a Bose-Einstein condensate in a time-dependent triple-well trap: Nonlinear eigenstates, Landau-Zener models, and stimulated Raman adiabatic passage," Phys. Rev. A **73**, 013617 (2006).
38. Xin Jiang, Li-Bin Fu, Wen-shan Duan and Jie Liu, "Phase transition of the ground state for two-component BoseEinstein condensates in a triple-well trap" Journal of Phys. B, **44**, 115301 (2011).
39. B. Liu, L. B. Fu, S. P. Yang, and J. Liu, "Josephson oscillation and transition to self-trapping for Bose-Einstein condensates in a triple-well trap," Phys. Rev. A. **75**, 033601 (2007).
40. C. J. Bradly, M. Rab, A. D. Greentree, and A. M. Martin, "Coherent tunneling via adiabatic passage in a three-well Bose-Hubbard system," Phys. Rev. A. **85**, 053609 (2012).
41. P. Jason, M. Johansson, and K. Kirr, "Quantum signatures of an oscillatory instability in the Bose-Hubbard trimer," Phys. Rev. E **86**, 016214 (2012).

#211632 - $15.00 USD Received 8 May 2014; revised 16 Jul 2014; accepted 17 Jul 2014; published 31 Jul 2014

42. P. Buonsante, R. Franzosi, and V. Penna, "Dynamical Instability in a Trimeric Chain of Interacting Bose-Einstein Condensates," Phy. Rev. Lett. **90**, 050404 (2003).
43. P. Buonsante, R. Franzosi and V. Penna, "Control of unstable macroscopic oscillations in the dynamics of three coupled Bose condensates," J. Phys. A. **42**, 285307 (2009).
44. V. Penna, "Dynamics of the central-depleted-well regime in the open Bose-Hubbard trimer," Phys. Rev. E **87**, 052909 (2013).
45. T. F. Viscondi and K. Furuya, "Dynamics of a BoseEinstein condensate in a symmetric triple-well trap," J. Phys. A. **44**, 175301 (2011).
46. H. Hennig, J. Dorignac, and D. K. Campbell, "Transfer of Bose-Einstein condensates through discrete breathers in an optical lattice," Phys. Rev. A. **82**, 053604 (2010).
47. K. Nemoto, C. A. Holmes, G. J. Milburn, and W. J. Munro, "Quantum dynamics of three coupled atomic Bose-Einstein condensates," Phys. Rev. A. **63**, 013604 (2000).
48. C.L Pando L. and E. J. Doedel, "1/f noise in a thin stochastic layer described by the discrete nonlinear Schrdinger equation," Phys. Rev. E **75**, 016213 (2007).
49. A. R. Kolovsky, "Semiclassical Quantization of the Bogoliubov Spectrum," Phys. Rev. Lett. **99**, 020401 (2007).
50. R. Franzosi and V. Penna, "Chaotic behavior, collective modes, and self-trapping in the dynamics of three coupled Bose-Einstein condensates," Phys. Rev. E. **67**, 046227 (2003).
51. M. Hiller, T. Kottos, and T. Geisel, "Complexity in parametric Bose-Hubbard Hamiltonians and structural analysis of eigenstates," Phys. Rev. A **73**, 061604(R) (2006).
52. R. Franzosi and V. Penna, "Self-trapping mechanisms in the dynamics of three coupled Bose-Einstein condensates," Phys. Rev. A. **65**, 013601 (2001).
53. M. Hiller, T. Kottos, and T. Geisel, "Wave-packet dynamics in energy space of a chaotic trimeric Bose-Hubbard system," Phys. Rev. A **79**, 023621 (2009).
54. M. Johansson, "Hamiltonian Hopf bifurcations in the discrete nonlinear Schrdinger trimer: oscillatory instabilities, quasi-periodic solutions and a 'new' type of self-trapping transition," J. Phys. A: Math. Gen. **37**, 2201–2222 (2004).
55. A. H. Castro Neto, F. Guinea, N. M. R. Peres, K. S. Novoselov, and A. K. Geim, "The electronic properties of graphene," Rev. Mod. Phys. **81**, 109–162 (2009).
56. Z. Chen and B. Wu, "Bose-Einstein condensate in a honeycomb optical lattice: fingerprint of superfluidity at the dirac point," Phys. Rev. Lett. **107**, 065301 (2011).
57. A. J. Lichtenberg and M. A. Lieberman, *Regular and stochastic Motion* (ASpringer-Verlag, New York) p. 1983B.
58. B. Wu and J. Liu, "Commutability between the Semiclassical and Adiabatic Limits," Phys. Rev. Lett. **96**, 020405 (2006).
59. A. Szameit, Y. V. Kartashov, M. Heinrich, F. Dreisow, R. Keil, S. Nolte, A. Tünnermann, V. A. Vysloukh, F. Lederer, and L. Torner, "Nonlinearity-induced broadening of resonances in dynamically modulated couplers," Opt. Lett. **34**, 2700–2702 (2009).
60. K. Henderson, C. Ryu, C. MacCormick, and M. G. Boshier, "Experimental demonstration of painting arbitrary and dynamic potentials for BoseEinstein condensates," New J. Phys. **11**, 043030 (2009).
61. J. Koch and K. L. Hur, "Discontinuous current-phase relations in small one-dimensional Josephson junction arrays," Phy. Rev. L **101**, 097007 (2008)
62. X. B. Luo, L. P. Li, L. You and B. Wu, "Coherent destruction of tunneling and dark Floquet state," New J. Phys. **16**, 013007 (2014)
63. L. Dell Anna, G. Mazzarella, V. Penna, and L. Salasnich, "Entanglement entropy and macroscopic quantum states with dipolar bosons in a triple-well potential," Phys. Rev. A **87**, 053620 (2013).
64. T. Lahaye, T. Pfau, and L. Santos, "Mesoscopic ensembles of polar Bosons in triple-well potentials," Phys. Rev. Lett. **104**, 170404 (2010).

1. Introduction

A Bose-Einstein condensate (BEC) is an ideal platform, where many interesting nonlinear dynamics and macroscopic tunneling phenomena can be studied in well-controlled simple settings [1–9]. Although these phenomena can also be studied in other systems, for example, superconductors and nonlinear waveguides, BECs offer certain unique advantages. For macroscopic tunneling, nonlinear effects can be explored in a BEC double-well system while it is impossible in a superconducting Josephson junction [10]. In a BEC system, the particle number can be well controlled, which allows people to study the semiclassical relation between quantum dynamics and nonlinear dynamics. In the nonlinear waveguide system, this is impossible as the photon number has to be large enough to ensure nonlinearity of the system.

A BEC in a double-well potential is probably the most studied system along this direc-

#211632 - $15.00 USD Received 8 May 2014; revised 16 Jul 2014; accepted 17 Jul 2014; published 31 Jul 2014

tion [8–25]. Many interesting phenomena are found both theoretically and experimentally, e.g., Landau-Zener dynamics [11–15], macroscopic self-trapping [10, 16], the quantum and thermal fluctuations of the phase [17], atome interferometry [18], and double wells on atoms chips [19, 20] . This double-well BEC system was also studied by using both the mean-field model (the Gross-Pitaevskii equation) and the second-quantized model. The semiclassical relation between these models was explored and discussed [21]. Similar results have been found in a periodically-driving double-well BEC system in 2007 [22].

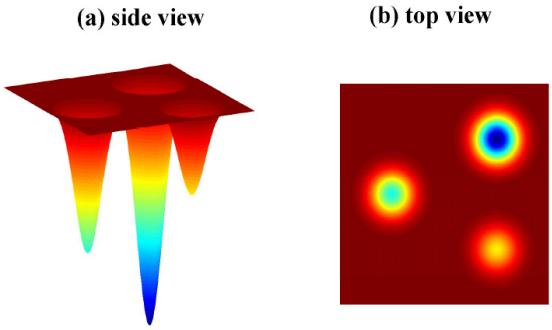

Fig. 1. Illustration of a potential with three mutually coupled wells.

Recently people have begun to study a BEC in a triple-well potential (or three weakly coupled BECs) with the expectation of discovery of more interesting phenomena [26–28]. There are two types of triple-well potentials, chain-shaped and ring-shaped. For the former, the three wells are aligned along a straight line with no coupling between the first and the third wells. For the latter, the three wells are on a ring and there is coupling between every pair of these wells (see Fig. 1). The chain-shaped triple-well is the focus of the most of these previous studies [26–41]. They found quantum signatures of the trimer model [40, 41], chaos behavior [42–44], off-site interaction [45], and discrete breather-phonon collisions [46]. In comparison, much less study has been done for the ring-shaped triple well [47–49]. Still people have found many interesting phenomena, the chaos behavior [50, 51], self-trapping [52], and the energy redistribution of interacting bosons in a ring-shaped quantum trimer [53]. The unstable regimes with repulsive [50] and attractive [54] both has also been investigated.

In this paper we focus on a BEC in a ring-shaped triple-well potential. Different from the ring-shaped model in [50] where the three wells are equal in depth, the depth of each well in our model can be tuned. As the well depths are changed, the three eigen-energies will form a band. When there is no interaction between the atoms, the two of the three eigen-energies become degenerate at the equal well-depth and form a Dirac point. This is due to that this ring-shaped model has the same symmetry as the graphene has around its K point [55, 56]. In comparison, for a BEC in a chain-shaped triple-well potential , it has no such a symmetry and there is no Dirac point [39]. As a result, we expect more interesting phenomena. In particular, we will use the second-quantized model to analyze the tunneling dynamics for this triple well system.

With the mean-field model, we find that the Dirac point is easily destroyed and developed into a loop structure with arbitrary small interaction. This is different from the double-well BEC system and the chain-shaped triple-well system, where the loop is formed only the interaction is big enough. The tunneling dynamics with a linearly sweeping field is also studied. We find that the tunneling dynamics is strongly influenced by the loop structure and the tunneling probability

#211632 - $15.00 USD Received 8 May 2014; revised 16 Jul 2014; accepted 17 Jul 2014; published 31 Jul 2014

is very sensitive to the system parameter, changing abruptly when the interaction strength is only slightly modified. This large erratic oscillation of tunneling probabilities with interaction strength can be attributed to the chaotic nature of the system.

For comparison, this triple-well BEC system is also studied with the second-quantized model. The second quantized energy levels are computed and compared to the mean-field levels. In the double-well BEC system, the mean-field energy levels encompasses a region where the second-quantized energy levels has avoided-crossings. Such a clear and simple correspondence is not found in this triple-well BEC system. In the second quantized model, the tunneling probabilities with a sweeping field are also found to change erratically with large amplitude as the interaction strength increasing. In the second quantized model, this erratic tunneling behavior can be attributed to that the positions of the avoided crossings in the energy spectrum depends sensitively on the system parameter. This result gives us some indication how the chaotic behavior in the mean-field model is related to the corresponding second-quantized energy levels.

This paper is organized as follows. In Sec. II, we present the mean-field model for our triple-well BEC system. Then we study the chaotic dynamics in this model and its influence on the tunneling results. In Sec. III, we use the fully quantized method to investigate the same system and make a comparison with the mean-field results. Sec. IV is a summary.

2. Mean field model

We consider a BEC residing in a triple-well potential, where the three wells are coupled with each other (see Fig. 1). We take the three-mode approximation and use a_1, a_2, a_3 to denote the probability amplitudes of a BEC residing in the three potential wells, respectively. This three-mode approximation is equivalently a single-band approximation: this approximation is good as long as the inter-well tunneling and the on-site interaction is much smaller than the energy gap. In this triple well system, the energy gap is roughly the gap between the ground state and the first-excited state in a single well.

We have made some assumptions to treat this model system in a three mode approximation [50]: The potential here is a symmetric ring-shaped triple well potential and the lowest energy level of each well is well separated from the higher energy levels. The interaction between particles is not strong enough to change this property of the system configuration. With the mean field approach, we then have the following dimensionless Schrödinger equation [47, 50, 56],

$$i\frac{\partial}{\partial t}\begin{pmatrix} a_1 \\ a_2 \\ a_3 \end{pmatrix} = H(\gamma)\begin{pmatrix} a_1 \\ a_2 \\ a_3 \end{pmatrix}. \tag{1}$$

with

$$H(\gamma) = \begin{pmatrix} -c|a_1|^2+\gamma & v/2 & v/2 \\ v/2 & -c|a_2|^2 & v/2 \\ v/2 & v/2 & -c|a_3|^2-\gamma \end{pmatrix}. \tag{2}$$

where $c > 0$ is the nonlinear interaction strength between bosons. The minus sign before c indicates that the interaction in the system is attractive. The coupling term v is chosen to be positive. 2γ denotes the energy offset between the first and third wells. The total probability $|a_1|^2+|a_2|^2+|a_3|^2$ is conserved to be 1. v is the coupling parameter. The corresponding energy of the system is $E = \gamma(|a_1|^2-|a_3|^2)+\frac{v}{2}(a_1^*a_2+a_1^*a_3+a_2^*a_1+a_2^*a_3+a_3^*a_1+a_3^*a_2)-c/2(|a_1|^4+|a_2|^4+|a_3|^4)$. The relation between the chemical potential and E is $E = \mu-\frac{c}{2}(|a_1|^4+|a_2|^4+|a_3|^4)$ where μ is the chemical potential defined as $\langle\psi|H|\psi\rangle$. One can use the well-known

#211632 - $15.00 USD Received 8 May 2014; revised 16 Jul 2014; accepted 17 Jul 2014; published 31 Jul 2014

procedure to find how these dimensionless parameters are related to the physical parameters in experiments [12, 21]. Note that the total number of the particles N is conserved in this system.

When $c = 0$, the system becomes a linear three-level system. Its energy spectrum with respect to the energy offset γ can be computed easily by diagonalizing the matrix in Eq. (2) . As shown in Figs. 2(a), there exists a Dirac point at $\gamma = 0$ in the energy band, similar to the Dirac point found in the Bloch bands of graphene. We find that this Dirac point is immediately destroyed once c becomes non-zero. As shown in Figs. 2(b), the Dirac point is replaced immediately by a sophisticated loop structure with a very small c. With the nonlinear parameter c increasing, the loop will maitain its topological structure but cover a larger region. That means the number of the fixed points will remain the same with the increase of the nonlinearity at $\gamma = 0$. This is in stark contrast with the chain-shaped model [39], where the loop appears only beyond a critical value of c. The mean field levels in Figs. 2 are computed by searching the solution of Eq. (1) of the form $a_j(\gamma,t) = a_j(\gamma)e^{-i\mu t}(j = 1,2,3)$.

The emergence of a loop structure in Figs. 2 with an infinitesimal small value of c can be shown analytically as we can find analytical solutions for the mean-field levels at $\gamma = 0$. These solutions can be grouped into four, which are marked by A, B, C, D in Figs. 2(d). The solutions

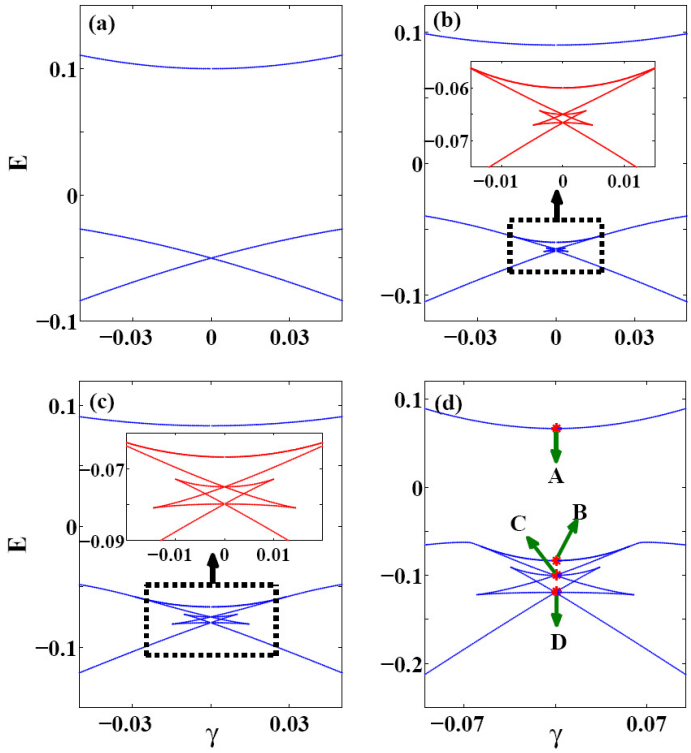

Fig. 2. Mean-field energy levels at $v = 0.1$ for different c. (a) $c = 0$; (b) $c = 0.06$; (c) $c = 0.1$; (d) $c = 0.2$.

#211632 - $15.00 USD Received 8 May 2014; revised 16 Jul 2014; accepted 17 Jul 2014; published 31 Jul 2014

at points A and B are

$$(a_1,a_2,a_3)_A = (\frac{1}{\sqrt{3}},\frac{1}{\sqrt{3}},\frac{1}{\sqrt{3}}), \tag{3a}$$

$$\mu_A = v - \frac{c}{3}; \tag{3b}$$

$$(a_1,a_2,a_3)_B = (\frac{1}{\sqrt{3}},-\frac{1}{2\sqrt{3}} \pm \frac{1}{2}i,-\frac{1}{2\sqrt{3}} \mp \frac{1}{2}i), \tag{3c}$$

$$\mu_B = -\frac{c}{3} - \frac{v}{2}. \tag{3d}$$

These solutions originate clearly from the linear solutions at $c = 0$. The solutions at point C are

$$(a_1,a_2,a_3)_C = (0, b+fi, -b-fi), \tag{4a}$$

$$\mu_C = -\frac{c+v}{2}. \tag{4b}$$

Here b, f can be any real number satisfying the condition $b^2 + f^2 = 1/2$. This means that there are infinite solutions at point C. The solutions of the lowest energy at point D are

$$(a_1,a_2,a_3)_D = (a, a, \sqrt{1-2a^2}), \tag{5a}$$

$$\mu_D = -ca^2 + v(a+\sqrt{1-2a^2})/(2a), \tag{5b}$$

where a is the roots of the equation $(av/2 - 3ca^3 + ca)\sqrt{1-2a^2} + v/2 - 2va^2 = 0$ which satisfies the conditions that a is real and $a \neq 1/\sqrt{3}$. One can prove without much difficulty that $(av/2 - 3ca^3 + ca)\sqrt{1-2a^2} + v/2 - 2va^2 = 0$ always has a real root $a \neq 1/\sqrt{3}$.

These solutions at C, D do not exist at $c = 0$ and emerge immediately when c is not zero. This proves analytically that the loop seen Figs. 2 appears at a infinitesimal value of c.

We are interested in the tunneling dynamics of this system when the level bias γ changes with time as $\gamma = \alpha t$. Here we focus on the adiabatic limit, that is, the sweeping rate α tends to zero. Due to the existence of Dirac point, it is impossible to establish the adiabatic criterion. In our numerical simulation, we choose $\alpha = 0.0001$. This sweeping rate is adiabatic for the corresponding two-model and the chain model. We always start with a state on the lowest branch of the levels and evolve the state according to Eq. (1) with γ changing from a large negative value to a large positive value at rate α. At the end, we compute how each well is populated $P = (P_1, P_2, P_3)$, where $P_i = |a_i|^2$. These populations P_i's are the end results of the tunneling under a sweeping field γ. When $c = 0$, during the adiabatic evolution the particles pass through the Dirac point, then move up to the second level. So, the final state will be $P_1 \simeq P_3 \simeq 0, P_2 \simeq 1$. When c increases, the Dirac point is destroyed and develops into a loop structure as shown in Figs. 2(b)-2(d). The loop will block the particles moving onto the second level, rendering a result significantly different from that for the case $c = 0$. This analysis is confirmed by our numerical results shown in Fig. 3, where the curves change rapidly with arbitrary small interaction.

One surprising feature in Fig. 3 is the large oscillations of P, which indicates that the tunneling dynamics in this system is very sensitive to the interaction c. This is not seen in the double-well system. In the following, we investigate the chaotic behavior of the system and find that it is the cause of the drastic oscillations. Here we use the method of Poincaré section [57].

It is more convenient to study chaos in the language of classical Hamiltonian. For this purpose, we transform this model mathematically into a classical Hamiltonian system with a well-known method [57]. We introduce $n_1 = |a_1|^2$, $n_2 = |a_2|^2$, $n_3 = |a_3|^2$, $\theta_1 = \arg a_2 - \arg a_1$, and

#211632 - $15.00 USD Received 8 May 2014; revised 16 Jul 2014; accepted 17 Jul 2014; published 31 Jul 2014

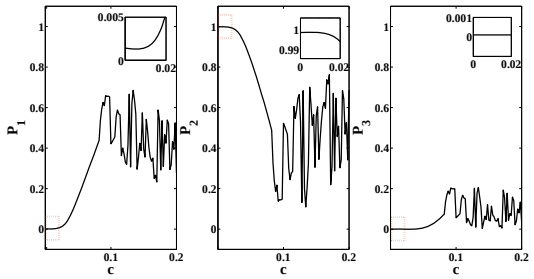

Fig. 3. Mean particle numbers of three wells as a function of c at $v = 0.1$. The sweeping rate is $\alpha = 0.0001$. P_i denotes the mean particle number in the ith well. The insets are the enlargement of the sections indicated in dashed boxes.

$\theta_3 = \arg a_2 - \arg a_3$. With the constraint $n_1 + n_2 + n_3 = 1$ and ignoring a total phase, we obtain a classical Josephson Hamiltonian,

$$\begin{aligned} H &= -c/2[n_1^2 + n_3^2 + n_2^2] - \gamma(n_1 - n_3) \\ &\quad + v\sqrt{n_1 n_2}\cos\theta_1 + v\sqrt{n_2 n_3}\cos\theta_3 \\ &\quad + v\sqrt{n_1 n_3}\cos(\theta_3 - \theta_1). \end{aligned} \tag{6}$$

The corresponding canonical equations of motion can be found in appendix A.

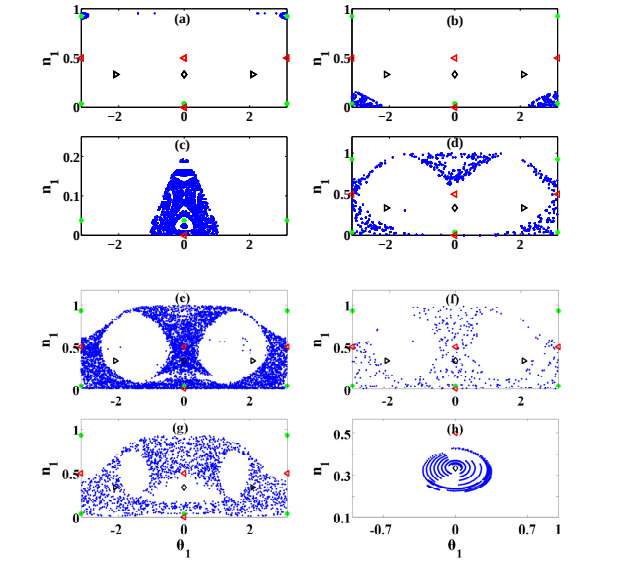

Fig. 4. The Poincaré sections at $\theta_3 = 0$ for $\gamma = 0.008, c = 0.2, v = 0.1$ with different energies E. (a) $E = -0.1215$, (b) $E = -0.1144$, (c) $E = -0.1103$, (d) $E = -0.1019$, (e) $E = -0.0975$, (f) $E = -0.0939$, (g) $E = -0.0780$, (h) $E = 0.0628$. The green stars are for energy level D in Fig. 2, the red triangles (left) are for C, the black triangles (right) for B, and the black diamonds for A.

The Poincaré section(PS) [39, 50, 57] is used to investigate the chaotic dynamics of this system. We only concentrate on the dynamics of the atoms whose energy is almost near the

#211632 - $15.00 USD Received 8 May 2014; revised 16 Jul 2014; accepted 17 Jul 2014; published 31 Jul 2014

eigenenergy of each fixed point and at the point of $\gamma = 0.008$ not far away from $\gamma = 0$. After taking a small perturbation on the eigenenergy of each level and setting $c = 0.2, v = 0.1$, we solve Eq. (5) numerically and select the PS by setting $\theta_3 = 0$, $d\theta_3/dt > 0$. The energy of each PS is fixed. The PSs from the lowest to the highest levels are shown in Fig. 4. Figs. 4(a),4(b),4(c) and 4(h) show that the motions around the levels that are connected to points A and D are rather regular while the motions for other levels as shown in Figs.4 (d)-4(g) are quite chaotic.

The numerical results in Fig. 4 clearly indicate that there exists chaotic behavior in our three-mode system. We find that the chaotic behavior persists as long as γ is not large. As γ sweeps, the system will have to go through this chaotic region and, therefore, the tunneling dynamics will be greatly influenced. This chaotic dynamical behavior is the cause for the large oscillations seen in Fig. 3. To illustrate this point more clearly, we have done another two sets of numerical calculations.

In the first set of calculations, we show that the tunneling dynamics is very sensitive to the choice of the initial state. The system parameters for this set of calculations are $c = 0.14, v = 0.1$. We choose one initial state as the eigenstate $\psi_0 = [a_1, a_2, a_3]$ at $\gamma = -3$ and the other initial state by taking a small perturbation of ψ_0, that is $\psi_0^{'} = \psi_0 + \delta_\psi$. δ_ψ is so small that the initial probability changes only around 10^{-4}. The state $|\psi(t)|^2$ at each step of the adiabatic evolution is recorded with $\gamma = \alpha t$ $(\alpha = 0.0001)$ and plotted in Fig. 5. In Figs. 5(a), we see that the initial state with the probabilities $P_{10} = 0.0001, P_{20} = 0.0002, P_{30} = 0.9997$ evolves to a state with $P_1 = 0.3868, P_2 = 0.6050, P_3 = 0.0082$. In Figs. 5(b), a slightly different initial state with $P_{10} = 0.0001, P_{20} = 0.0004, P_{30} = 0.9995$ will evolve to a state with $P_1 = 0.6093, P_2 = 0.2149, P_3 = 0.1758$, which is very different from the former result. These results show that, although the external condition is the same, a small perturbation to the initial state will make the results totally different. This means the tunneling dynamics of this system is very sensitive to the initial condition, which is a characteristics of chaotic behavior.

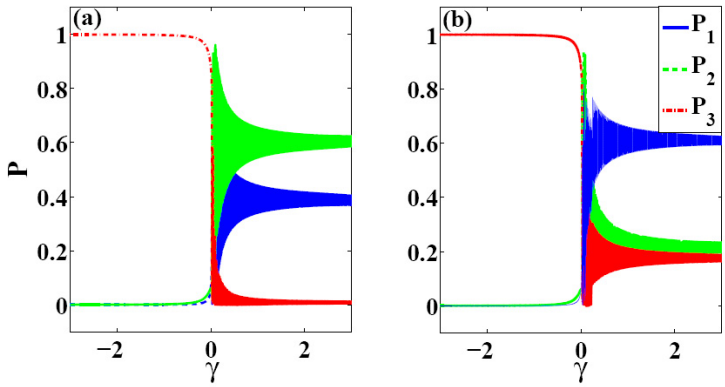

Fig. 5. The dynamic evolution of the particle numbers $P_i = |\psi(t)_i|^2$ in each well. Blue solid line indicates P_1, green dashed line is P_2, red dash dotted line corresponds to P_3, we use $c = 0.14, v = 0.1$. (a) The initial state is the lowest eigenstate at $\gamma = -3$; (b) The initial state is a small perturbation to the initial state in (a). The final mean particle numbers in the three wells are very different, indicating that a small change in the initial condition can cause a big change in the final state.

In the second set of calculations, we show that the tunneling dynamics is also sensitive to the system parameters. We focus on the interaction strength c. In Fig. 6, we use the eigenstates $\psi_0 = [a_1, a_2, a_3]$ at $\gamma = -3$ as the initial state for (a) $c = 0.12, v = 0.1$ and (b) $c = 0.14, v = 0.1$. We record $|\psi(t)|^2$ at each step of adiabatic evolution with $\gamma = \alpha t (\alpha = 0.0001)$. In Figs. 6 (a) $(c = 0.12, v = 0.1)$, the initial probabilities are $P_{10} = 0.0001, P_{20} = 0.0002, P_{30} = 0.9997$.

#211632 - $15.00 USD Received 8 May 2014; revised 16 Jul 2014; accepted 17 Jul 2014; published 31 Jul 2014

After the adiabatic evolution, they become $P_1 = 0.4553, P_2 = 0.4948, P_3 = 0.0499$. In Figs. 6(b) ($c = 0.14, v = 0.1$), the initial probabilities are $P_{10} = 0.0001, P_{20} = 0.0002, P_{30} = 0.9997$, and they become $P_1 = 0.3868, P_2 = 0.6050, P_3 = 0.0082$, very different from the former result. The comparison indicates that the tunneling probability changes abruptly when the interaction strength is modified only slightly .

The sensitivity to the initial conditions and system parameters that we have shown can only be explained with the chaotic behavior of the system near $\gamma = 0$ seen in Fig. 4. When the system evolves to the region near $\gamma = 0$, the small difference will be magnified by the chaotic behavior and lead to very different end results as indicated by the large oscillations in Fig. 3.

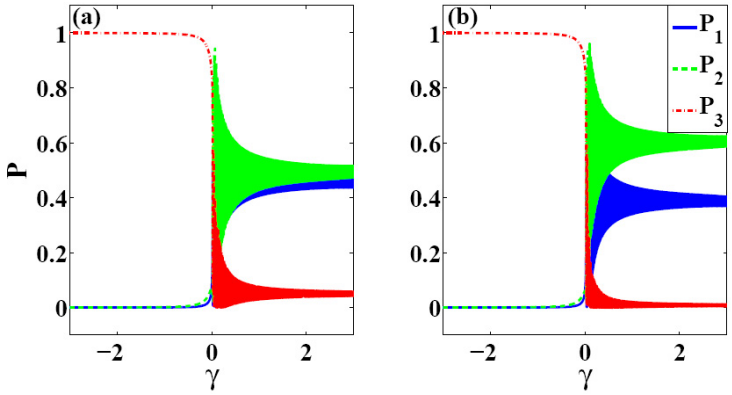

Fig. 6. Mean particle numbers of three wells during the adiabatic evolution of γ. The adiabatic rate is $\alpha = 0.0001$. The initial condition is the lowest eigenstate at $\gamma = -3$. (a) $v = 0.1, c = 0.12$; (b) $v = 0.1, c = 0.14$. The final probabilities in the three wells are very different, indicating that a small change in the system parameters can also cause a large change in the final state.

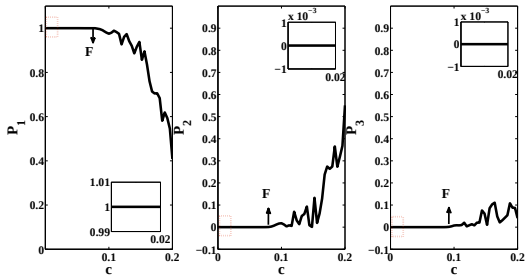

Fig. 7. Mean particle numbers as a function of c in a chain-shaped three-well system [39]. $v = 0.1, \alpha = 0.0001$. The critical point is labeled by red point F, the critical value of c is around $c = 0.076$. The insets are the enlargement of the sections indicated in dashed boxes.

It is important to compare our ring-shaped system to a chain-shaped system, where there is no coupling between the first well and the third well [39, 42–44]. For the chain model, the Hamiltonian has the following form,

$$H = \begin{pmatrix} -c|a_1|^2 + \gamma & v/2 & 0 \\ v/2 & -c|a_2|^2 & v/2 \\ 0 & v/2 & -c|a_3|^2 - \gamma \end{pmatrix}. \quad (7)$$

#211632 - $15.00 USD Received 8 May 2014; revised 16 Jul 2014; accepted 17 Jul 2014; published 31 Jul 2014

There is no Dirac point at $c = 0$ for this system and the loop structure emerges only beyond a critical value of c [39]. Our computation shows that this feature will lead to a different tunneling dynamics. As shown in Fig. 7, especially the zoomed parts in the figure, the populations at the three wells at the end of tunneling are not sensitive to the interaction strength c and remain almost flat before a critical value of c (the red point F in Fig. 7). This is obviously different from the ring model, where the tunneling is strongly affected by small interaction (see Fig. 3). On the other hand, we also notice a common feature between Fig. 3 and Fig. 7: there are large oscillations in the tunneling when c is large. They are caused by chaos near $\gamma = 0$ in both models. In [39], the chaos in the chain model was found to have a great effect on the tunneling dynamics.

So far we have assumed that c, v are fixed while γ is changing. In fact, for a BEC in a triple-well potential, c and v will also change when γ changes. Nevertheless, these change will not significantly alter our main results. In the experiment [11] where the tunneling dynamics in a double-well BEC system is studied, their results agree well with the two-mode model where c, v are fixed while γ is changing [12]. There are various ways to realize our model in experiments. In fact, this type of ring-shaped optical lattices with an arbitrary number of sites has been achieved in 2009 [60]. Our model can also be realized with an internal Josephson junction employing three spin-states of Bose-Einstein condensate [61]. Furthermore, our model can realized with a BEC system in a honeycomb lattice [56] and the nonlinear wave guide system [22, 59]. In the last two systems, γ can indeed be varied with c, v fixed.

3. Second quantized model

This triple-well BEC system can be also described by a second-quantized Hamiltonian, which is

$$\begin{aligned}\hat{H} = &-\gamma(\hat{a}_1^\dagger\hat{a}_1 - \hat{a}_3^\dagger\hat{a}_3) + v/2(\hat{a}_1^\dagger\hat{a}_2 + \hat{a}_2^\dagger\hat{a}_1 + \hat{a}_2^\dagger\hat{a}_3 \\ &+ \hat{a}_3^\dagger a_2 + a_3^\dagger a_1 + a_1^\dagger a_3) - c/(2N)(\hat{a}_1^\dagger\hat{a}_1^\dagger\hat{a}_1\hat{a}_1 \\ &+ \hat{a}_2^\dagger\hat{a}_2^\dagger\hat{a}_2\hat{a}_2 + \hat{a}_3^\dagger\hat{a}_3^\dagger\hat{a}_3\hat{a}_3). \end{aligned} \tag{8}$$

where $\hat{a}_i^\dagger$, $\hat{a}_i (i = 1, 2, 3)$ are the generators and annihilators for the quantum states at the three wells. The mean-field model (2) is an approximation in the large N limit. In the following, we shall study the energy levels and tunneling dynamics in this second quantized model and compare them to the mean-field results.

The energy levels of the second-quantized mode (8) can be found by directly diagonalizing the Hamiltonian $\hat{H}$ and are plotted in Fig. 9 as the blue lines. Many avoided-crossings with tiny gaps appear in the lower part of the quantized energy levels with the increase of the mean-field interaction c. These avoided-crossings were also found in [50, 51].

The mean-field energy levels (red circles) are also plotted in Fig. 9 for comparison. We see that the quantized energy levels are bounded by the mean-field levels from the bottom and the top. We also notice that the mean-field loop structure overlaps very much with the region in the quantized energy levels, where the avoided-crossings with tiny gaps concentrate.

This kind of comparison between the mean-field energy levels and the quantized ones has been done for a double-well BEC system [58]. The Sommerfeld quantization method is used in [21] to analyse the mean field and the quantized theory. However, in our case the Sommerfeld quantization procedure can not be applied because the three-mode system studied here is chaotic and not integrable [42–44]. Einstein was believed to be the first one to notice this.

For convenient comparison, we have plotted the double-well results in Figs. 10(a), where one sees that the avoided-crossings in the quantized levels are enveloped by the mean-field energy levels. This prominent feature is not seen in our three-mode BEC system (see Figs. 10(b,c)).

#211632 - $15.00 USD Received 8 May 2014; revised 16 Jul 2014; accepted 17 Jul 2014; published 31 Jul 2014

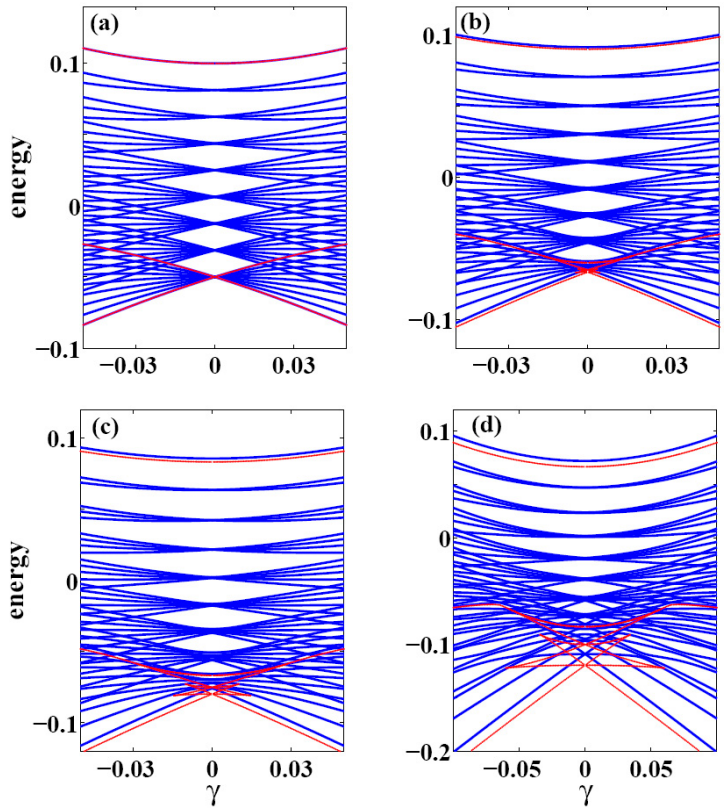

Fig. 8. Energy levels from the second-quantized model for different c: (a) $c = 0$, (b) $c = 0.06$, (c) $c = 0.1$, (d) $c = 0.2$. The red circles are for the mean-field energy levels; the blue lines stand for the quantized levels. $N = 8,\ v = 0.1$

As clearly seen in Figs. 10(c), for our three-mode system, there are many avoided-crossings outside the loop. This difference may be caused by the chaos in the three-mode system.

We now use this second quantized model to study the tunneling dynamics. Similarly, we set the initial state ϕ_0 in the lowest level. The system evolves as γ sweeps slowly across $\gamma = 0$ with a given rate α $(\alpha = 0.0001)$. The dynamic evolution of $\phi(t)$ is recorded. At the end, we calculate the particle numbers in each well: $P_i = \left\langle \phi(t)|\hat{a}_i^{\dagger}\hat{a}_i|\phi(t)\right\rangle, (i = 1,2,3)$. The results are plotted in Fig. 11, where the mean-field results from Fig. 4 are also plotted for comparison. The green, red, and black stars are for the quantized results at $N = 8, 10, 15$, respectively. Due to the limit of our computing capability, we can not compute for larger particle numbers.

As seen in Fig. 11, the quantized tunneling results agree well with the mean-field results. When c is small, there is almost perfect agreement between the two. In the region where c is big and the mean-field results oscillate greatly, the quantized results change erratically with the interaction strength but with a much smaller amplitude than the mean-field one.

To have a better understanding of the erratic oscillation in the quantized results, we track how the probability $A_i = |\langle\phi_i|\phi_t\rangle|^2$ on the ith level changes with time. ϕ_i is the eigenstate for the ith level and ϕ_t is the time evolution of ϕ_0. In Fig. 12, the first, second, and third largest A_i are recorded using black, green, and red stars. It is quite clear that these stars do not stay on the same levels and keep switching levels at avoided crossings. Only at large γ, these colored stars will remain on their respective levels without further switching. In Figs. 12(a) for $c = 0.12, v = 0.1$, the largest three probabilities at the end are on the 11th, 7th, and 6th levels in the descending

#211632 - $15.00 USD Received 8 May 2014; revised 16 Jul 2014; accepted 17 Jul 2014; published 31 Jul 2014

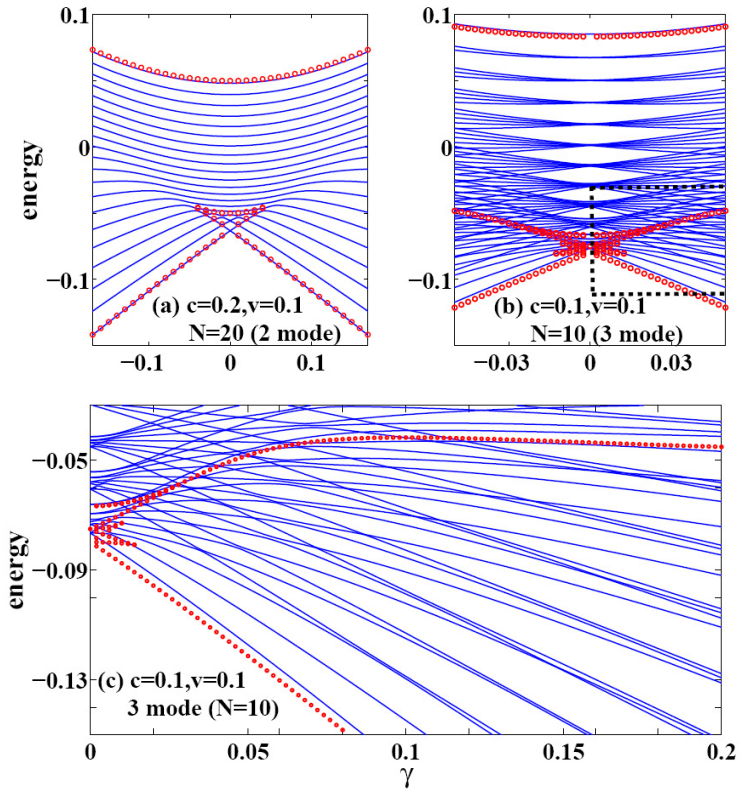

Fig. 9. Energy levels from the second-quantized model (blue solid lines) and mean-field model (red open circles) for a double-well model and the ring-shaped triple-well model. (a) The energy levels for two-mode model for $N = 20, c = 0.4, v = 0.2$, the quantized hamiltonian of this model is $\hat{H} = \gamma(\hat{a}_1^\dagger \hat{a}_1 - \hat{a}_2^\dagger \hat{a}_2)/2 + v(\hat{a}_1^\dagger \hat{a}_2 + \hat{a}_1 \hat{a}_2^\dagger)/2 - c(\hat{a}_1^\dagger \hat{a}_1 - \hat{a}_2^\dagger \hat{a}_2)^2/(4N))$ [13]. (b) The energy levels for the ring-shaped triple-well energy for $N = 10, c = 0.1, v = 0.1$. (c) The enlarged rectangle part in (b). In (a), all the avoided-crossing points are enveloped in the mean-field energy levels. In (b,c), this is not the case; many avoided-crossing points lie outside of the envelope of the mean-field energy levels.

order. With a slight change of parameters to $c = 0.14, v = 0.1$, the largest three become the 7th, 8th, and 11th levels as seen in Figs. 12(b), apparently different from the case in Figs. 12(a). This kind of change of levels and their ordering can lead to large change of tunneling between wells. In Figs. 12(c,d), we have plotted how the populations on these energy levels evolve with time. We see many sharp changes, which are caused by the tunneling at avoided-crossings with tiny energy gaps.

Table 1. The mean particle number P_i in each well at different energy levels. The parameters are $\gamma = 0.4, N = 8, c = 0.12, v = 0.1$

	6_{th}	7_{th}	8_{th}	9_{th}	10_{th}	11_{th}	12_{th}
P_1	0.6169	0.7414	0.4942	0.6164	0.3718	0.6168	0.4945
P_2	0.3755	0.0116	0.4965	0.2549	0.6184	0.1337	0.3739
P_3	0.0076	0.2470	0.0093	0.1287	0.0098	0.2495	0.1216

In Table 1 and 2, we have listed the populations $P_i (i = 1, 2, 3) = \langle \phi_n | \hat{a}_i^\dagger \hat{a}_i | \phi_n \rangle$ at each well for

#211632 - $15.00 USD Received 8 May 2014; revised 16 Jul 2014; accepted 17 Jul 2014; published 31 Jul 2014

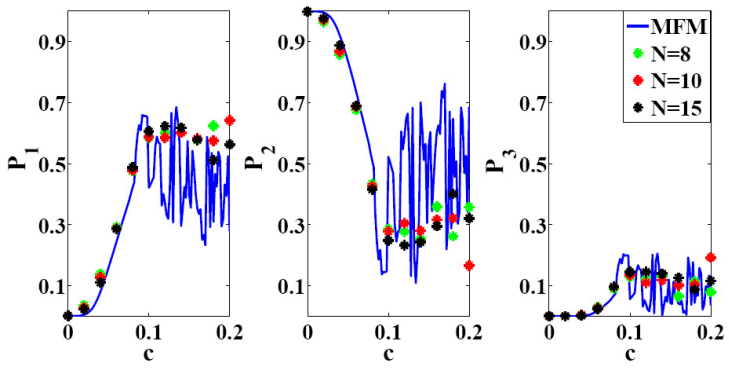

Fig. 10. Mean particle numbers as a function of c for $v = 0.1$ in the ring-shaped triple-well model. $v = 0.1, \alpha = 0.0001$. The solid lines are for the mean-field model; the green, red and black stars are the quantized results for $N = 8, 10, 15$, respectively.

Table 2. The mean particle number P_i in each well at different energy levels. The parameters are $\gamma = 0.4, N = 8, c = 0.14, v = 0.1$

	6_{th}	7_{th}	8_{th}	9_{th}	10_{th}	11_{th}	12_{th}
P_1	0.6165	0.7417	0.4935	0.6163	0.3709	0.6169	0.4940
P_2	0.3761	0.0113	0.4975	0.2550	0.6197	0.1333	0.3744
P_3	0.0073	0.2470	0.0090	0.1288	0.0094	0.2498	0.1316

different eigenstates ϕ_n. It is clear from the two tables that the population P_i at each well for a given eigenstate does not change much with a slight change of system parameters. However, P_i can change greatly between neighboring eigenstates.

With these detailed information that we have presented, it is not hard to understand the erratic oscillations seen in Fig. 11. With a small change of system parameters, the positions of the avoided-crossing will change. Although this shift of the avoided-crossing positions is small, it will affect which pairs of energy levels undergo the tunneling first, and will eventually affect which energy levels have the largest occupation probabilities and the number of particles in each well according to Table I, II. With this picture in mind, we expect that the fluctuations will increase with the number of particle N. With the increase of particle number N, the number of the avoid crossings will also increase. As a result, the tunneling between avoided crossings will be more sensitive to the system parameters; this will leads to greater fluctuations of the particle number in each well. Unfortunately, we are not able to verify this as our limit of computational power. This analysis gives us some indication how the chaotic behavior in the mean-field model is related to the structures in the corresponding second-quantized energy spectrum.

We emphasize that our model can also be used to describe a BEC system in a honeycomb lattice near point **K** [56], and be applied in nonlinear waveguide systems [22,59]. As the optical triple waveguides can be easily built in experiment, the tunneling dynamics that we found in the mean-field model can be easily observed experimentally [59, 62].

4. Conclusion

In summary, we have investigated the tunneling dynamics of three BECs which are coupled to each other weakly. This is done with both the mean-filed model and the second-quantized model. Our results show that a loop structure appears in the mean-field energy bands immediately after the interaction is turned on. This is accompanied by the appearance of avoided-

#211632 - $15.00 USD Received 8 May 2014; revised 16 Jul 2014; accepted 17 Jul 2014; published 31 Jul 2014

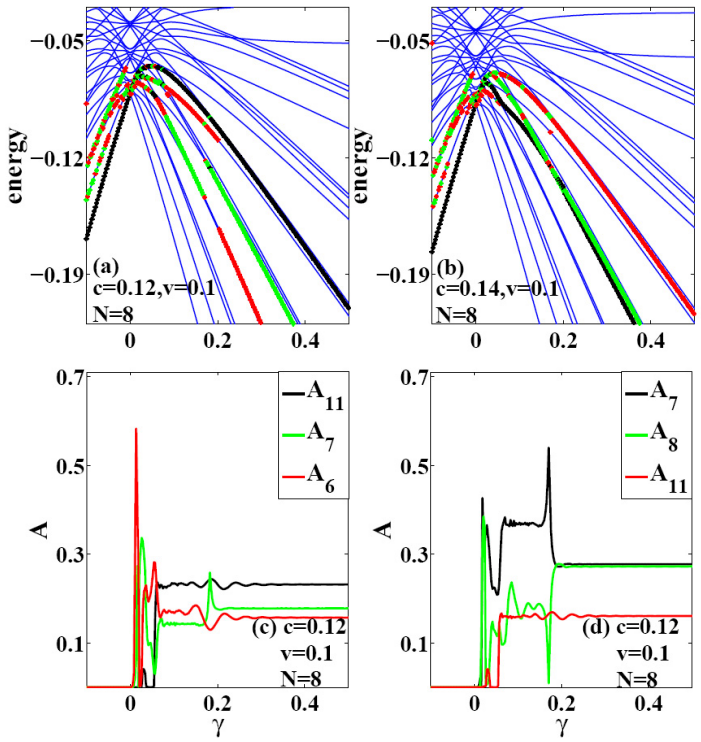

Fig. 11. The probability A_i of the i_{th} level ($A_i = \langle\phi_i|\phi_t\rangle$). In (a,b), the first, second, and third largest A_i during the evolution are traced with black, green, and red stars, respectively, on the energy levels. (a) $c = 0.12, N = 8, v = 0.1$; (b) $c = 0.14, N = 8, v = 0.1$. (c) The time evolution of A_{11} (black), A_7(green), A_6 (red) for the case of (a). (d) The time evolution of A_7 (black), A_8(green), A_{11} (red) for the case of (b). The sharp peaks in (c) and (d) are caused by the avoided-crossings.

crossings in the corresponding second-quantized levels. We have also found that the tunneling dynamics in this system is very sensitive to the system parameter, e.g., the interaction strength. In the mean-field approach, the chaotic behavior in the system is found to be responsible for this sensitivity. In the second-quantized model, this sensitivity is found to be related to the concentration of large number of avoided crossings near $\gamma = 0$.

Our analysis can be easily extended to many other interesting cases, for example, the repulsive interaction and the dipole interaction [63, 64]. For the latter, the off-site interaction can become important and it is interesting to see how the tunneling dynamics is affected by the off-site interaction. More importantly, we plan to carry out more detailed analysis to explore the corresponding relation between the quantum and classical chaos with this model in the future research.

Appendix

A. The canonical equations of motion

Let $n_1 = |a_1|^2$, $n_2 = |a_2|^2$, $n_3 = |a_3|^2$, $\theta_1 = \arg a_2 - \arg a_1$, and $\theta_3 = \arg a_2 - \arg a_3$. With the constraint $n_1 + n_2 + n_3 = 1$ and ignoring a total phase, we obtain a classical Josephson Hamil-

#211632 - $15.00 USD Received 8 May 2014; revised 16 Jul 2014; accepted 17 Jul 2014; published 31 Jul 2014

tonian,

$$\begin{aligned} H &= -c/2[n_1^2+n_3^2+n_2^2]-\gamma(n_1-n_3) \\ &\quad +v\sqrt{n_1n_2}\cos\theta_1+v\sqrt{n_2n_3}\cos\theta_3 \\ &\quad +v\sqrt{n_1n_3}\cos(\theta_3-\theta_1). \end{aligned} \tag{9}$$

Considering $n_2 = 1-n_1-n_3$, then

$$\begin{aligned} H &= -c/2[1+2n_1^2+2n_3^2+2n_1n_3-2(n_1+n_3)] \\ &\quad -\gamma(n_1-n_3)+v\sqrt{n_1(1-n_1-n_3)}\cos\theta_1 \\ &\quad +v\sqrt{n_3(1-n_1-n_3)}\cos\theta_3 \\ &\quad +v\sqrt{n_1n_3}\cos(\theta_3-\theta_1). \end{aligned} \tag{10}$$

Here $\{n_1,\theta_1\}$ and $\{n_3,\theta_3\}$ are two pairs of canonical variables. So $\frac{dn_j}{dt}=-\frac{\partial H}{\partial\theta_j}$, $\frac{d\theta_j}{dt}=\frac{\partial H}{\partial n_j}$:

$$\frac{dn_3}{dt} = v\sqrt{n_3n_2}\sin\theta_3+v\sqrt{n_1n_3}\sin(\theta_3-\theta_1), \tag{11a}$$

$$\begin{aligned} \frac{d\theta_3}{dt} &= -c(n_3-n_2)+\gamma+\frac{v\sqrt{n_2}}{2\sqrt{n_3}}\cos\theta_3 \\ &\quad -\frac{v}{2\sqrt{n_2}}(\sqrt{n_1}\cos\theta_1+\sqrt{n_3}\cos\theta_3) \\ &\quad +\frac{n_1}{2\sqrt{n_1n_3}}v\cos(\theta_3-\theta_1), \end{aligned} \tag{11b}$$

$$\frac{dn_1}{dt} = v\sqrt{n_1n_2}\sin\theta_1+v\sqrt{n_1n_3}\sin(\theta_3-\theta_1), \tag{11c}$$

$$\begin{aligned} \frac{d\theta_1}{dt} &= -c(n_1-n_2)-\gamma+\frac{v\sqrt{n_2}}{2\sqrt{n_3}}\cos\theta_1 \\ &\quad -\frac{v}{2\sqrt{n_2}}(\sqrt{n_1}\cos\theta_1+\sqrt{n_3}\cos\theta_3) \\ &\quad +\frac{n_3}{2\sqrt{n_1n_3}}v\cos(\theta_3-\theta_1). \end{aligned} \tag{11d}$$

where $\{n_1,\theta_1\}$ and $\{n_3,\theta_3\}$ are two pairs of canonical variables.

Acknowledgment

This work is supported by the National Fundamental Research Program of China under Grant No. 2011CB921501, No. 2012CB921300, No. 2013CB921900; the National Natural Science Foundation of China under Grant No. 61078026, No. 10934010, No. 91336103, No. 11274024, and No. 11334001.